

Implications of non-Markovian dynamics on information-driven engine

Obinna Abah^{1,*} and Mauro Paternostro^{1,†}

¹*Centre for Theoretical Atomic, Molecular and Optical Physics,
School of Mathematics and Physics, Queen's University Belfast, Belfast BT7 1NN, United Kingdom*

The understanding of memory effects arising from the interaction between system and environment is a key for engineering quantum thermodynamic devices beyond the standard Markovian limit. We study the performance of measurement-based thermal machine whose working medium dynamics is subject to backflow of information from the reservoir via collision based model. In this study, the non-Markovian effect is introduced by allowing for additional unitary interactions between the environments. We present two strategies of realizing non-Markovian dynamics and study their influence on the work produced by the engine. Moreover, the role of system-environment memory effects on the engine performance can be beneficial in short time.

I. INTRODUCTION

The second law of thermodynamics is ubiquitous in nature: it stipulates that heat always flows from hot place to cold one. However, in 1867 Maxwell proposes the opposite with his idea of an intelligent demon to illustrate the statistical nature of the second law of thermodynamics [1]. The demon, with sufficiently information about the microscopic motions of individual atoms and molecules, is capable to separate the fast-moving (“hot”) ones from the slow-moving (“cold”) ones and induce the heat to flow from cold to hot, in apparent contradiction with the second law of thermodynamics. It took nearly a century to resolve this apparent paradox following a series of works, starting from Szilard’s engine [2] through Landauer [3], Bennett [4] and others to clarify the link between the information recorded by the demon and the thermodynamic entropy, see [5]. The advances in nanotechnology have made the realization of Maxwell’s thought experiment, Szilard’s engine possible in recent time [6–9].

In addition to this, there has been a parallel line of development in the non-Markovian dynamic behavior of system interacting with reservoir. Theoretical advances have been made on its characterization [10–12] as well as verifications [13–15] in various experimental setup. The role of memory (non-Markovian) effects in understanding of information processing at both the classical and quantum level is currently attracting research interest [16–19]. Recently, studying the non-Markovian dynamic of a system has shed more light into the understanding of the Landauer principle [18].

Over the past few years, great effort has been devoted on studying the interplay between thermodynamics and quantum mechanics [20–25]. Remarkable progress has been made in understanding the non-equilibrium processes in thermodynamics [26] as well as extending/generalizing the second law of thermodynamics to incorporates measurement and feedback driven processes [27–34]. Recently, the role of feedback control on information thermodynamic engine has been experimentally studied in different platform [35–40]. However, the understanding of the machine performance when

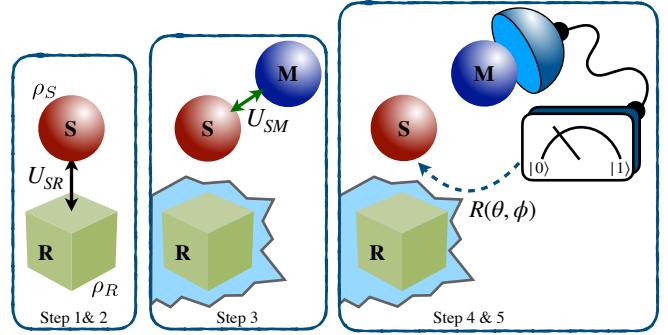


FIG. 1. The various steps of the general protocol that we consider. The jagged light-blue area stands for the tracing-out of the environmental system. The information-gathering process in Step 3 consists of a projective measurement performed on the state of the ancilla M , which is projected onto the elements of its computational basis, such as $\{|0\rangle_M, |1\rangle_M\}$ in the case of a qubit.

the feedback engine protocol is performed by system exhibiting non-Markovian dynamics is still lacking. Although the self-consistent formulation of an interpretation of thermodynamic laws in the presence of measurements and feedback is still work in progress, and is attracting much attention, more practical issues such as the enhancement of the performance of cooling algorithms by feedback-based mechanisms are already under investigation and exploitation [41–44].

In this paper, we investigate the implications of non-Markovian dynamics on feedback information-driven machines. Our findings show that memory effect can enhance the overall performance of the engine in a short time. The rest of the paper is organized as follows. In the next section, Section II, we first present the description of the measurement-based engine and then briefly discuss its thermodynamic analysis. In Section III we introduce the collision based model of realizing non-Markovian dynamics and outline example of two different strategies. Then, the characterization of the non-Markovian features is numerical analyze in Section IV A, while the analysis of the feedback-driven engine in both Markovian and non-Markovian situation is devoted to Section IV B. Finally, Section V draws our conclusions.

* o.abah@qub.ac.uk

† m.paternostro@qub.ac.uk

II. MEASUREMENT-BASED THERMO-MACHINE

The system initially prepared in given state is brought to contact with a heat reservoir. Then, the system is decoupled and attached to a measuring apparatus initially prepared in a given state. The apparatus determine the state of the system and depending on the result of the measurement, a feedback operation is performed on the system. The setup consists of three components; system, reservoir and an ancilla.

A. Description of the protocol

We now introduce and illustrate the protocol that we aim at studying for the investigation of the effects that a process of information-gathering and feedback have on the capability of the system to perform work. We proceed step by step, as follows:

Step 1: Initial preparation.– System S and thermal reservoir(s) R are prepared in their respective equilibrium states at inverse temperature $\beta_i = 1/k_B T_i$ and frequency ω_i , where $i = S, R$. The initial system-reservoir state is described by the density matrix

$$\rho_{SR} = \bigotimes_{j=R,S} \rho_j = \bigotimes_{i=R,S} \frac{e^{-\beta_i H_i}}{Z_i}, \quad (1)$$

where H_i denotes the Hamiltonian of element i and $Z_i = \text{tr} [e^{-\beta_i H_i}]$ is the corresponding partition function. For simplicity, we will consider the case in which the system and the reservoir are made of two-level systems.

Step 2: System-environment coupling.– System and reservoir interact unitarily. In line with the usual formalism used in collisional models for quantum open-system dynamics [34, 45–50], in what follows we will concentrate on a time-evolution operator of the partial-SWAP form such as

$$U_{SR} = e^{-i\tau} [\cos(2\tau)\mathbb{1}_4 + i \sin(2\tau)U_{sw}], \quad (2)$$

where τ is a dimensionless interaction time and U_{sw} is the two-particle SWAP transformation $|i, j\rangle_{SR} \xrightarrow{U_{sw}} |j, i\rangle_{SR}$ with $|i\rangle_S [|j\rangle_R]$ a state of the computational basis chosen for S [R].

The S - R state after such unitary evolution is thus

$$\rho_{SR}^u = U_{SR}(\rho_S \otimes \rho_R)U_{SR}^\dagger. \quad (3)$$

In general, the joint dynamics embodied by U_{SR} gives rise to quantum correlations between system and environment. The environment is then discarded, leaving us with the reduced state of the system only

$$\rho_S^u = \text{tr}_R [\rho_{SR}^u]. \quad (4)$$

Step 3: Pre-measurement.– The system is then brought into contact with a measuring apparatus, i.e. an ancillary qubit M prepared in state ρ_M . The S - M coupling takes place according to the unitary transformation U_{SM} , which gives the joint density matrix

$$\rho_{SM}^{pm} = U_{SM}(\rho_S^u \otimes \rho_M)U_{SM}^\dagger. \quad (5)$$

We assume that U_{SM} takes place over a dimensionless interaction time τ_m and that the corresponding coupling Hamiltonian H_{SM} such that $U_{SM} = e^{-i\tau_m H_{SM}}$ takes the form of a spin-spin coupling $H_{SM} = \sigma_S^{(i)} \otimes \sigma_M^{(i)}$, whose form will be specified later on. Here, $\sigma_j^{(i)}$ is the $i = x, y, z$ Pauli spin operator of particle $j = S, M$.

Step 4: Measurement.– This is the actual information-gathering step where the information on S acquired by the ancilla during Step 3 through their mutual interaction is inferred via an actual measurement process. The latter is described by the complete set of projective operators $\{M_M^{(k)}\}$, defined in the Hilbert space of the ancilla M . Let us assume that the ancilla is initially prepared in one of its computational-basis states, i.e. $\rho_M = |p\rangle\langle p|_M$. The probability that outcome k is obtained as a result of such measurement is given by

$$P_k = \text{tr}_{SM} [M_M^{(k)} \rho_{SM}^{pm} M_M^{(k)}] = \text{tr}_S [\mathcal{F}_k \rho_S^u] \quad (6)$$

with $\mathcal{F}_k = \mathcal{E}_k^\dagger \mathcal{E}_k$ and $\mathcal{E}_k = {}_M \langle k | U_{SM} | p \rangle_M$ an element of the positive-operator value measure (POVM) induced on the system. The corresponding post-measurement state of the system reads

$$\rho_S^k = \frac{\mathcal{E}_k \rho_S^u \mathcal{E}_k^\dagger}{P_k}. \quad (7)$$

Step 5: Feedback control operation.– Based on the outcome of the measurement at Step 4, the controller performs a conditional operation on the state of the system [27, 31]. The most general unitary transformation on a single-qubit state is a rotation by an angle α about an arbitrary axis identified by the unit vector $\mathbf{n} = (\sin \theta \cos \phi, \sin \theta \sin \phi, \cos \theta)$, which has been written in polar coordinates specified by the polar angle θ and azimuthal one ϕ . By including a general global phase γ , such rotation reads

$$R(\mathbf{v}) = e^{i\gamma} \begin{pmatrix} \cos \frac{\alpha}{2} - i \cos \theta \sin \frac{\alpha}{2} & -i \sin \frac{\alpha}{2} \sin \theta e^{-i\phi} \\ \sin \frac{\alpha}{2} \sin \theta e^{i\phi} & \cos \frac{\alpha}{2} + i \cos \theta \sin \frac{\alpha}{2} \end{pmatrix} \quad (8)$$

with $\mathbf{v} := (\gamma, \alpha, \theta, \phi)$. In our case, the set of parameters upon which such rotation depends should be interpreted as conditioned on the outcome of the measurement performed, at Step 4, on the ancilla M . That is

$$\mathbf{v} \longrightarrow \mathbf{v}_k := (\gamma_k, \alpha_k, \theta_k, \phi_k). \quad (9)$$

The use of such conditioned rotation, which embodies our simple feedback control operation, delivers the state of the system

$$\rho_S^{fb} = R(\mathbf{v}_k) \rho_S^k R^\dagger(\mathbf{v}_k). \quad (10)$$

Step 6: Final state and reset.– The system evolve independently and a fresh ancilla is made available to the next iteration of the protocol, which proceeds again from Step 1 onwards. This stage has no effect on the analysis that follows.

B. Thermodynamics of the machine

We proceed with the thermodynamic analysis of the protocol presented above, by calculating the changes in internal

energy $E[\rho] \equiv \text{tr}[H\rho]$ and entropy $S[\rho] \equiv -k_B \text{tr}[\rho \ln \rho]$ of the system associated with the preparation, measurement and feedback-control protocols.

First, after the system preparation (interaction with the reservoir), the change in the internal energy is

$$\Delta E^u = E[\rho_S^u] - E[\rho_S] = \text{tr}[H_S \rho_S^u] - \text{tr}[H_S \rho_S], \quad (11)$$

and the change in system entropy reads

$$\Delta S^u = S[\rho_S^u] - S[\rho_S] = -k_B \left(\text{tr}[\rho_S^u \ln \rho_S^u] - \text{tr}[\rho_S \ln \rho_S] \right). \quad (12)$$

From the first law of thermodynamics, the work done on/by the system in light of the change of its energy is $\Delta W^u = \Delta E^u - \Delta S^u/T$, where we used the relation $\Delta S = T\Delta Q$, which associates a change in the entropy of the system occurring in light of the exchange of heat ΔQ with its environment.

For the measurement step, the thermodynamic quantities are as follows. The variation of internal energy of the system reads

$$\Delta E^{pm} = E[\rho_S^{pm}] - E[\rho_S^u] = \text{tr}[H_S \rho_S^{pm}] - \text{tr}[H_S \rho_S^u], \quad (13)$$

where $\rho_S^{pm} = \text{tr}_M[\rho_{SM}^{pm}]$ is the reduced state of the system after the pre-measurement step (cf. Step 3). The corresponding change in entropy of the state of the system is

$$\Delta S^{pm} = S[\rho_S^{pm}] - S[\rho_S^u] = -\beta_S \left(\text{tr}[\rho_S^{pm} \ln \rho_S^{pm}] - \text{tr}[\rho_S^u \ln \rho_S^u] \right). \quad (14)$$

Any process involving energy dissipation in the form of heat being exchanged with an environment leads to an irreversible increase of entropy [29]. Based on the second law of phenomenological non-equilibrium thermodynamics, the entropy production characterizing the irreversibility of the measurement process is given by the sum of the entropy change in the system and in the measurement apparatus (environment). The entropy production is non-negative and reads [51, 52]

$$\begin{aligned} \Sigma^{pm} &= \Delta S_{SM}^{pm} - \beta_S \Delta Q^{pm} \\ &= \Delta S_S^{pm} + \Delta S_M^{pm} - I_{S:M}^{pm} - \beta_S \Delta Q^{pm} \geq 0. \end{aligned} \quad (15)$$

The first two terms in Eq. (15) correspond to the change in entropy of the system and the ancilla, while the third term is the quantum mutual information between them. On the other hand, from the first law, we have $\Delta E^{pm} = \Delta W^{pm} + \Delta Q^{pm}$. Combining these equations, we can find that the work extracted from the system following the measurement that we have performed is bounded by a quantity that depends on the amount of information that the ancilla gathered on S as quantified by the mutual information. Specifically, we have

$$-\beta_S W^m \leq -\beta_S \Delta E^{pm} + \Delta S_S^{pm} + \Delta S_M^{pm} - I_{S:M}^{pm}. \quad (16)$$

Then, during the feedback step, the variation of system energy and entropy are

$$\begin{aligned} \Delta E^{fb} &= E[\rho_S^{fb}] - E[\rho_S^{pm}] = \text{tr}[H_S \rho_S^{fb}] - \text{tr}[H_S \rho_S^{pm}], \\ \Delta S^{fb} &= S[\rho_S^{fb}] - S[\rho_S^{pm}], \end{aligned} \quad (17)$$

respectively. Here definitions analogous to those used above hold for both $S[\rho_S^{fb}]$ and $S[\rho_S^{pm}]$. Using again the first and second laws, we have

$$\Delta E^{fb} = \Delta W^{fb} + \Delta Q^{fb}, \quad \Sigma^{fb} = \Delta S^{fb} - \Delta Q^{fb} \geq 0, \quad (18)$$

where we note that the feedback protocol can be engineered so as to change only the system density matrix and leave that of the ancilla unaffected. This is possible, for instance, by post-selecting only the measurement events where the state of the ancilla is found to be the initially prepared one $|p\rangle_M$. We can thus establish an upper bound to the amount of thermodynamic work extracted by the feedback protocol as

$$-\beta_S W^{fb} \leq -\beta_S \Delta E^{fb} + \Delta S^{fb}. \quad (19)$$

By combining Eqs. (16) and (19), the total work extracted through the protocol that we are considering reads

$$\begin{aligned} -\beta_S W_{tot} &= -\beta_S (W^m + W^{fb}) \\ &\leq \beta_S (\Delta F_S^{pm} + \Delta F_S^{fb}) + \Delta S_M^{pm} - I_{S:M}^{pm}, \end{aligned} \quad (20)$$

where we have defined the difference in free energy between the initial and the final states of the system during one of the steps of the protocol as $\Delta F_S \equiv \Delta E - T\Delta S$. The bound in Eq. (20) is the modified second law of thermodynamics in the presence of feedback control. The form of such bound provided by Sagawa and Ueda in Ref. [27] is recovered in the case that the measurement process does not influence the measurement apparatus, that is $\Delta S_M^{pm} = 0$. For more discussion on the subject, see Ref. [34]. Considering that, in our protocol (cf. step 6), system and controller are reset to their initial state at the end of each measurement process, we have that ΔF remains invariant (namely $\Delta F_S^{mi} + \Delta F_S^{fi} = 0$) and

$$-\beta_S W_{tot} \leq \Delta S_M^{pm} - I_{S:M}^{pm}. \quad (21)$$

In spirit of an earlier approach [29, 53], a well-motivated identification of energetic efficiency of a feedback controlled system is the ratio of the mean extractable work to the mean information acquired through measurement. Thus, the efficiency based on Eq. (21) can be written as

$$\eta = \frac{\beta_S W_{tot}}{I_{S:M}^{pm}} \leq 1 - \frac{\Delta S_M^{pm}}{I_{S:M}^{pm}}, \quad (22)$$

where in the case of unchanged the measurement apparatus we have $\Delta S_M^{pm} = 0$.

III. NON-MARKOVIAN DYNAMICS OF THE SYSTEM - COLLISIONAL BASED MODEL

Here, we consider a situation where the system undergoes non-Markovian dynamics as a result of its interaction with the environment (taking place at steps 1 and 2 of our protocol). The realization of the dynamics that we decide to consider is that of collisional models, which offer great flexibility and richness of phenomenology [49].

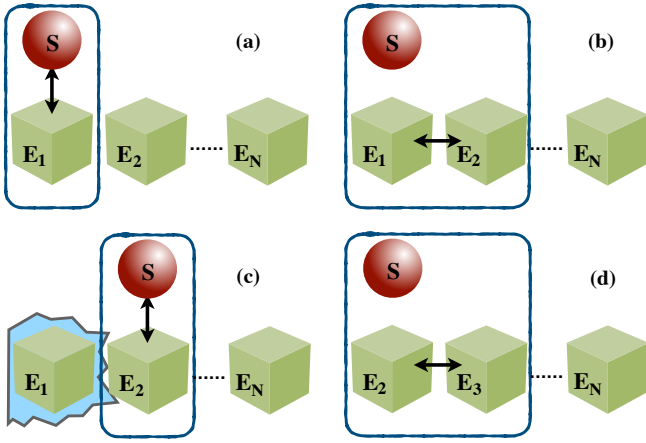


FIG. 2. Schematic of non-Markovian dynamics via collision model for nearest sub-environment collisions. The system and the sub-environment particles are initially uncorrelated. In the first step (a), the system S interacts with E_1 . The next step, (b) E_1 interacts with E_2 and thereby correlating the system and particles E_1 and E_2 . Then step (c), E_1 is traced away. After which the system interacts with E_2 before isolating the system for measurement and feedback processes in strategy 1. For the strategy 2, the system and sub-environment particles collisional iterations are performed up to E_3 , (a) - (d), before the measurement and feedback.

In particular, we consider the case in which the reservoir's memory mechanism arises from collisions between different elements of a structured, multi-party environment, following an interaction with the system. This scenario has been successfully used in the past to model memory-bearing mechanisms able to propagate to the environment information acquired on the state of the system [54]. More recently, this realization of memory-bearing effects has been used to assess the performance of a quantum Otto cycle having a harmonic system as a working medium [55]. Collisional models allow for the tracking of the dynamics of both system and environments, which in turn makes it possible to follow the ensuing emergence of the system-environment correlations responsible for memory effects [45, 47–49, 56, 57]. They are thus invaluable methodological tools to assess the back-action of memory-bearing environments on the information-driven engine at the core of our study.

As anticipated above, we assume an environment R made up of a large number of elements, which we label $\{E_1, E_2, \dots, E_n\}$ and assume, for the sake of simplicity, to be mutually identical. The total state of system and environment is initially factorized and the dynamics proceeds through as sequential collisions (interaction process) between S and an element E_n of the environment. These are followed by pairwise collisions/interactions between the elements of the environment, as illustrated in Fig. 2. In Ref. [54], it has been shown that the degree of non-Markovianity of the reduced system dynamics depends on how the erasure of system-environment correlations is performed.

Here, we will consider two inequivalent schemes of tracing out the degree of freedom of the environment. The first scenario that we consider to compute the reduced dynamics of S

requires the environmental particle E_n to be traced out when it has interacted with S and E_{n+1} but before the system interacts with E_{n+1} . In the second scenario, the system experiences pairwise interactions with the triplet (E_n, E_{n+1}, E_{n+2}) , interspersed by environment-environment interactions, after which the reduced state of the system is obtained, ready for its use in the engine protocol. We also assume that the environment-environment interaction evolution is described by the unitary operator [47–49]

$$U_{EE} = e^{-i\tau_e} [\cos(2\tau_e)\mathbb{1}_4 + i \sin(2\tau_e)U_{sw}], \quad (23)$$

which describes another partial-SWAP gate between two consecutive elements of the environment, parameterized by the dimensionless interaction time τ_e .

The first scenario (which we term *strategy-1*) that we consider involves tracing out the particle E_n after it has collided with E_{n+1} , as exemplified in Fig. 2 (a) - (c). It starts with a collision between S and E_n , modelled through the unitary operation U_{SR} in Eq. (2), which delivers the joint state

$$\rho_{SE_1} = U_{SR}(\rho_S \otimes \rho_{E_1})U_{SR}^\dagger. \quad (24)$$

The three particles S, E_n and E_{n+1} then become correlated through the intra-environment interaction $U_{E_n E_{n+1}}$ in Eq. (23), after which particle E_n is traced out. This results in the bipartite S - E_2 state

$$\rho_{SE_2} = \text{tr}_{E_1} [U_{EE}(\rho_{SE_1} \otimes \rho_{E_2})U_{EE}^\dagger]. \quad (25)$$

The marginal state of the system is computed after the interaction with E_{n+1} . Thus, *strategy-1* prepare the system in state

$$\rho_S^\mu = \text{tr}_{E_2} [U_{SR}\rho_{SE_2}U_{SR}^\dagger]. \quad (26)$$

At the end of the system-environment interaction, the engine-protocol steps [step 3 - 6] are performed before the system collides with another fresh environment.

In the second scenario, dubbed *strategy-2*, the system collides in a systematic fashion with the environmental components E_n, E_{n+1} , and E_{n+2} , see the illustration in Fig. 2 (a) - (d). The states achieved at each stage of *strategy-2* are thus as follows

$$\begin{aligned} \rho_{SE_1} &= U_{SR}(\rho_S \otimes \rho_{E_1})U_{SR}^\dagger, \\ \rho_{SE_2} &= \text{Tr}_{E_1} [U_{EE}(\rho_{SE_1} \otimes \rho_{E_2})U_{EE}^\dagger], \\ \rho_{SE_3} &= \text{Tr}_{E_2} [U_{EE}(U_{SR}\rho_{SE_2}U_{SR}^\dagger \otimes \rho_{E_3})U_{EE}^\dagger], \\ \rho_S^\mu &= \text{Tr}_{E_3} [\rho_{SE_3}]. \end{aligned} \quad (27)$$

This scenario clearly differs from the first one in both the number of particles being involved, and the amount of correlations that are retained as a result of the system-environment interaction. In turn, this influences the non-Markovian features of the dynamical maps applied to S and arising from the implementation of such strategies.

To quantify the degree of non-Markovianity of the reduced system dynamics undergone by S , we employ the measure for non-Markovianity proposed in Ref. [10] which is associated with back-flow of information from the environment to the

system. This is based on the time behavior of the trace distance between two different initial quantum states of S , that is

$$D(\rho_1, \rho_2) = \frac{1}{2} \|\rho_1 - \rho_2\|, \quad (28)$$

where $\|\rho\| = \text{tr}[\sqrt{\rho^\dagger \rho}]$ is the trace norm of operator ρ and $\rho_{1,2}$ are two density matrices of S . For Markovian dynamics, $D(\rho_1, \rho_2)$ monotonically decreases with time for any pair of initial states $\rho_{1,2}(0)$. On the contrary, a dynamical process is signalled as non-Markovian if there is a pair of such states for which this quantity exhibits a non-monotonic behaviour.

IV. ANALYSIS OF NON-MARKOVIANITY AND ITS ROLE IN THE PERFORMANCE OF THE ENGINE

Now we present the numerical analysis of the non-Markovian dynamics of the collision model for both strategies described above and then, their role on the thermodynamics of the engine. In the remainder of the paper, we will use the initial system or reservoir preparation determined by the Bloch sphere angle θ of the form

$$\rho_G(\theta) = \begin{pmatrix} \cos^2 \theta & \cos \theta \sin \theta \\ \cos \theta \sin \theta & \sin^2 \theta \end{pmatrix}, \quad \theta = \{0, \pi/2\}. \quad (29)$$

The two-level system/reservoir Hamiltonian can be written as $H_j = \omega_j \rho_G(\theta)/2$ and the resulting thermal state is given by

$$\rho_j(\theta) = \exp[-\beta_j H_j] / Z_j, \quad (30)$$

where $j = S, R$ and β_j is the inverse temperature of the system.

A. Non-Markovianity features from both strategies

We numerically analyze the behaviour of the trace distance $D(\rho_{S_1}, \rho_{S_2})$ as the collision-based model for system-environment interactions are repeatedly executed. Figure 3 show the differences between the two strategies addressed in this study. For purely Markovian dynamics, the trace distance decreases monotonously while switching on the inter-environment interactions results in revivals that are evidence of non-Markovianity. In fact, this system-environment interaction produces a backflow mechanism - which is seen as oscillations of the trace distance that fades out in the large number of collisions. While the non-Markovian dynamics persists for both strategies in strong intra-environment interaction, the intermediate coupling strength shows a clear dependence of the non-Markovian nature on the way information/correlation is developed via collisions. It can be seen that the oscillations are more frequent in *strategy-2* (Fig. 3**(b)**) but fades out faster than the oscillations of the *strategy-1*, see Fig. 3**(a)**. The strongly non-Markovian dynamics observed in both strategies occurs at full-swap condition, $\tau_e = \pi/4$.

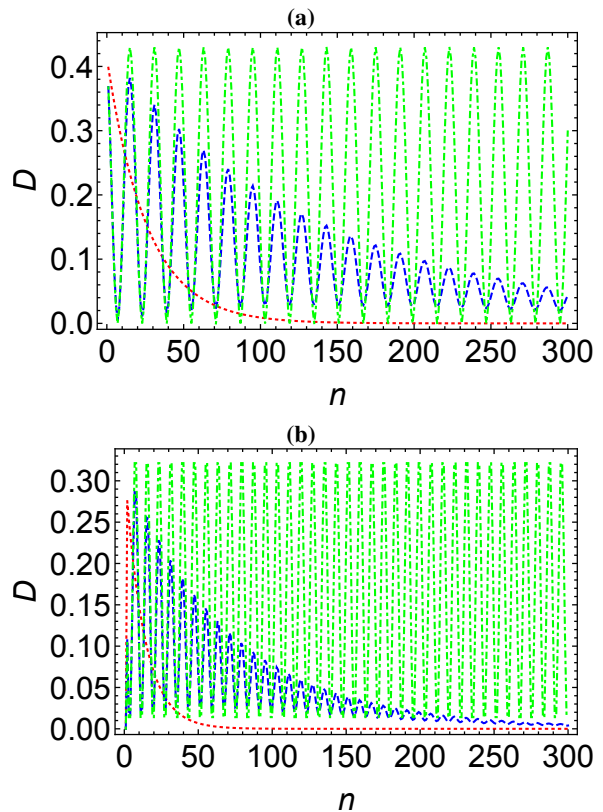


FIG. 3. The trace distance D between evolved system states as a function of the number of collision iteration n with the environment for both strategies. Upper **(a)** [lower **(b)**] panel are the results for the *strategy-1* [*strategy-2*]. We have considered the initial states $\rho_{S_1}(0)$ and $\rho_{S_2}(\pi/4)$, while the sub-environments are prepared in $\rho_R(\pi/2)$. The red dotted curve corresponds to the Markovian situation, $\tau_e = 0.0$, while the blue dashed and green dot-dashed curves represent the non-Markovian dynamics with the dimensionless inter-environmental coupling time $\tau_e = 10\pi/43$ and $\tau_e = \pi/4$ respectively. The system and environment frequency parameters are $\omega_s = 3$ and $\omega_r = 1$, while their inverse temperature is fixed at $\beta = 0.94$.

B. Feedback-driven engine analysis

Let now evaluate the influence of non-Markovianity on performance of the measurement-based machine described in section II above. We consider a two-level system initially prepared in the state $\rho_S(0)$ and many identical subenvironment prepared in the state $\rho_{E_n}(\pi/2)$. The measurement ancilla is prepared in the same state as the system with the system-measurement apparatus unitary evolution of the form $U_{SM} = \exp(-i\tau_m \sigma_x \otimes \sigma_x)$, where τ_m is the dimensionless system-probe interaction time. After a feedback operation is performed on the state of the system based on the outcome of the measurement, the thermodynamic quantities, work and quantum mutual information are numerically calculated, see Fig. 4. Note, in the numerics, the maximal values of the energy $E[\rho_S^{fb}]$ and entropy $S[\rho_S^{fb}]$ are obtained by optimization of the feedback rotation parameters $R(0, \alpha, \theta, \phi)$ from $0 - 2\pi$.

In Fig. 4, the feedback engine performance, work per-

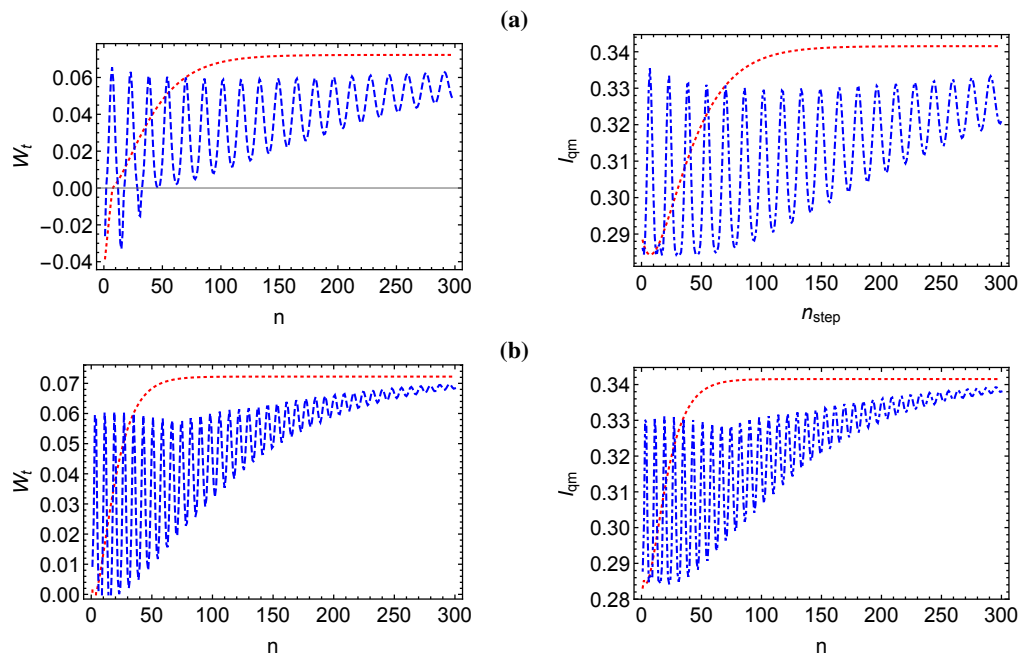


FIG. 4. Feedback driven engine performance: The total work performed W_t and the quantum mutual information I_{qm} as a function of number of collision n with the environment. The upper panel (a) corresponds to *strategy-1* while the lower panel (b) is for *strategy-2*. The red dotted curve corresponds to the Markovian dynamics, $\tau_e = 0.0$ while the blue dashed curve represent the non-Markovian dynamics, $\tau_e = 10\pi/43$. The system-environment interaction time is $\tau = \pi/32$ for weak coupling and the system and environment frequencies parameters are $\omega_s = 1$ and $\omega_r = 3.0$ respectively. The system-probe interaction time is $\tau_m = \pi/14$ and $\beta = 0.94$.

formed by the engine and the corresponding quantum mutual information associated with the measurement step, as a function of repeated collision are presented for the two different non-Markovian strategies described above. For the Markovian dynamics, the work and quantum mutual information increases as the system-environment interactions times grow until it they reach constant values in the after many collision iteration. As the system dynamics is prepared to be non-Markovian, an oscillatory behaviour which vanishes in the long collision time are observed for both engine performance quantities. These are true for both settings of non-Markovian strategies with the oscillations of *strategy-2* fading faster. This behaviour is akin to the observation in the trace distance fig. 3, in which the *strategy-2* oscillation are short time leave. The non-Markovian feature is strong at short collision times and can exceed their Markovian counterpart. However, the intermediate system-environment iteration is marked with suppression of the engine performance due to memory effect. At longer times, both strategies approach the performance under Markovian conditions, suggesting an eventual reduction of information back-flow. Moreover, the efficiency of information-to-work conversion Eq. (22) (figure not shown) exhibits similar behaviour as the two quantities presented.

V. CONCLUSION

We have investigated the interplay between memory effects and performance of a feedback-driven quantum engine. The engine setup consists of system, reservoir and measurement probe which have modelled as set of two-level systems. We have employed the trace distance as a measure of memory effects (non-Markovianity) to illustrate two strategies of realizing non-Markovian dynamics. We have observed that the memory effect can enhance the performance of feedback driven engine in a system-environment interaction short time. However, the performance decreases during the intermediate interaction time and approaches the Markovian value at very long time. Besides shedding light on the interplay between non-Markovianity and measurement driven engine, this study suggest more theoretical effort to understand the role of memory on information thermodynamics.

ACKNOWLEDGEMENT

The authors acknowledge the support by the Royal Society (Grant Numbers NF160966 and NI160057), the Royal Commission for the Exhibition of 1851, the SFI-DfE Investigator Programme grant (Grant 15/IA/2864), and the H2020 Collaborative Project TEQ (Grant Agreement 766900).

[1] H.S. Leff and A.F. Rex, *Maxwell's Demon 2: Entropy, Classical and Quantum Information, Computing* (Princeton Univer-

sity Press, Princeton, NJ, 2003).

- [2] L. Szilard, *Z. Phys.* **53**, 840 (1929).
- [3] R. Landauer, *IBM J. Res. Dev.* **5**, **183** (1961).
- [4] C.H. Bennett, *Int. J. Theor. Phys.* **21**, **905** (1982).
- [5] J.M.R. Parrondo, J.M. Horowitz, and T. Sagawa, *Nat. Phys.* **11**, **131** (2015).
- [6] S. Toyabe, T. Sagawa, M. Ueda, E. Muneyuki, and M. Sano, *Nature Phys.* **6**, 988 (2010).
- [7] A. Bérut, A. Arakelyan, A. Petrosyan, S. Ciliberto, R. Dillenschneider and E. Lutz, *Nature* **483** 187 (2012).
- [8] J.V. Koski, V.F. Maisi, J.P. Pekola, and D.V. Averin, *Proc. Natl. Acad. Sci. U.S.A.* **111**, 13786 (2014).
- [9] J.V. Koski, V.F. Maisi, T. Sagawa, and J.P. Pekola, *Phys. Rev. Lett.* **113**, 030601 (2014).
- [10] H-P. Breuer, E-M. Laine, and J. Piilo, *Phys. Rev. Lett.* **103**, 210401 (2009).
- [11] A. Rivas, S.F. Huelga and M.B. Plenio, *Phys. Rev. Lett.* **105**, 050403 (2010)
- [12] S.F. Lorenzo, F. Plastina and M. Paternostro, *Phys. Rev. A* **88**, 020102 (2013)
- [13] B-H. Liu, L. Li, Y-F. Huang, C-F. Li, G-C. Guo, E-M. Laine, H-P. Breuer, and J. Piilo, *Nature Phys.* **7**, 931
- [14] A.M. Souza, J. Li, D.O. Soares-Pinto, R.S. Sarthour, S. Oliveira, S.F. Huelga, M. Paternostro and F.L. Semião, arXiv:1308.5761 (2013)
- [15] A. Chiuri, C. Greganti, L. Mazzola, M. Paternostro and P. Mataloni, *Sci. Rep.* **2**, 968 (2012).
- [16] D. Reeb and M.M. Wolf, *New. J. Phys.* **16**, 103011 (2014)
- [17] S. Lorenzo, R. McCloskey, F. Ciccarello, M. Paternostro and G. M. Palma, *Phys. Rev. Lett.* **115**, 120403 (2015).
- [18] M. Pezzutto, M. Paternostro and Y. Omar, *New. J. Phys.* **18**, 123018 (2016).
- [19] S. Hamedani Raja, M. Borrelli, R. Schmidt, J. P. Pekola, S. Maniscalco, *Phys. Rev. A* **97**, 032133 (2017).
- [20] J. Gemmer, M. Michel, and G. Mahler, *Quantum Thermodynamics* (Springer, Berlin, 2004).
- [21] G. Huber, F. Schmidt-Kaler, S. Deffner, and E. Lutz, *Phys. Rev. Lett.* **101**, 070403 (2008).
- [22] M. Campisi, P. Hänggi, and P. Talkner, *Rev. Mod. Phys.* **83**, 771 (2011).
- [23] L. Mazzola, G. De Chiara, and M. Paternostro, *Phys. Rev. Lett.* **110**, 230602 (2013).
- [24] T.B. Batalhão, A.M. Souza, L. Mazzola, R. Auccaise, R.S. Sarthour, I.S. Oliveira, J. Goold, G. De Chiara, M. Paternostro, and R.M. Serra, *Phys. Rev. Lett.* **113**, 140601 (2014).
- [25] S. An, J.-N. Zhang, M. Um, D. Lv, Y. Lu, J. Zhang, Z.-Q. Yin, H.T. Quan, and K. Kim, *Nature Phys.* **11**, 193 (2015).
- [26] C. Jarzynski, *Ann. Rev. Cond. Mat. Phys.* **2**, 329 (2011).
- [27] T. Sagawa and M. Ueda, *Phys. Rev. Lett.* **100**, 080403 (2008).
- [28] T. Sagawa and M. Ueda, *Phys. Rev. Lett.* **104**, 090602 (2010).
- [29] K. Jacobs, *Phys. Rev. A* **80**, 012322 (2009).
- [30] S. Deffner, *Phys. Rev. E* **88**, 062128 (2013).
- [31] K. Funo, Y. Watanabe and M. Ueda, *Phys. Rev. E* **88**, 052121 (2013).
- [32] J.M. Horowitz and H. Sandberg, *New J. Phys.* **16**, 125007 (2014)
- [33] J. Goold, M. Huber, A. Riera, L. del Rio, and P. Skrzypczyk, *J. Phys. A* **49**, 143001 (2016).
- [34] P. Strasberg, G. Schaller, T. Brandes, and M. Esposito, *Phys. Rev. X* **7**, 021003 (2017).
- [35] P.A. Camati, J.P.S. Peterson, T.B. Batalhão, K. Micadei, A.M. Souza, R.S. Sarthour, I.S. Oliveira and R.M. Serra, *Phys. Rev. Lett.* **117**, 240502 (2016).
- [36] M. A. Ciampini, L. Mancino, A. Orioux, C. Vigliar, P. Mataloni, M. Paternostro, and M. Barbieri, *npj Quantum Information* **3**, 10 (2017).
- [37] N. Cottet, S. Jezouin, L. Bretheau, P. Campagne-Ibarcq, Q. Ficheux, J. Anders, A. Auffèves, R. Azouit, P. Rouchon, and B. Huard, *Proc. Natl. Acad. Sci.* **114**, 7561 (2017).
- [38] Y. Masuyama, K. Funo, Y. Murashita, A. Noguchi, S. Kono, Y. Tabuchi, R. Yamazaki, M. Ueda, and Y. Nakamura, arXiv:1709.00548 (2017).
- [39] T.P. Xiong, L.L. Yan, F. Zhou, K. Rehan, D.F. Liang, L. Chen, W.L. Yang, Z.H. Ma, M. Feng, and V. Vedral, *Phys. Rev. Lett.* **120**, 010601 (2018).
- [40] M. Naghiloo, J.J. Alonso, A. Romito, E. Lutz, and K.W. Murch, arXiv:1802.07205 (2018).
- [41] P.O. Boykin, T. Mor, V. Roychowdhury, F. Vatan, and R. Vrijen, *Proc. Natl. Acad. Sci.* **99**, 3388 (2002).
- [42] J. Baugh, O. Moussa, C.A. Ryan, A. Nayak, and R. Laflamme, *Nature* **438**, 470 (2005).
- [43] P. Liuzzo-Scorpo, L. A. Correa, R. Schmidt and G. Adesso, *Entropy* **18**, 48 (2016).
- [44] N.A. Rodríguez-Briones, E. Martín-Martínez, A. Kempf, and R. Laflamme, *Phys. Rev. Lett.* **119**, 050502 (2017).
- [45] V. Scarani, M. Ziman, P. Stelmachovic, N. Gisin, and V. Buzek, *Phys. Rev. Lett.* **88**, 097905 (2002).
- [46] M. Ziman, P. Stelmachovic, V. Buzek, M. Hillery, V. Scarani, N. Gisin, *Phys. Rev. A* **65**, 042105 (2002).
- [47] S. Lorenzo, R. McCloskey, F. Ciccarello, M. Paternostro, and G. M. Palma, *Phys. Rev. Lett.* **115**, 120403 (2015).
- [48] S. Kretschmer, K. Luoma, and W. T. Strunz, *Phys. Rev. A* **94**, 012106 (2016).
- [49] F. Ciccarello, *Quant. Meas. Quant. Metrol.* **4**, 53 (2017); F. Ciccarello and V. Giovannetti, *Phys. Scr.* **T153**, 014010 (2013).
- [50] S. Seah and S. Nimmrichter, arXiv:1809.04781 (2018).
- [51] M. Esposito, K. Lindenberg, and C. Van Den Broeck, *New J. Phys.* **12**, 013013 (2010)
- [52] S. Deffner and E. Lutz, *Phys. Rev. Lett.* **107**, 140404 (2011).
- [53] F.J. Cao and M. Feito, *Phys. Rev. E* **79**, 041118 (2009).
- [54] R. McCloskey and M. Paternostro, *Phys. Rev. A* **89**, 052120 (2014).
- [55] M. Pezzutto, M. Paternostro, and Y. Omar, *Quantum Sci. Technol.* **4**, 025002 (2019).
- [56] S. Campbell, F. Ciccarello, G.M. Palma, and B. Vacchini, *Phys. Rev. A* **98**, 012142 (2018).
- [57] B. Cakmak, S. Campbell, B. Vacchini, Ö.E. Müstecaplioglu, and M. Paternostro, *Phys. Rev. A* **99**, 012319 (2019).